

*Full Length Research Paper*

# **Geo-spatial distribution of radio refractivity and the influence of fade depth on microwave propagation signals over Nigeria**

**Olalekan Lawrence Ojo**

Department of Physics, University of Lagos, Yaba Akoka Lagos, Nigeria.

Received 30 June, 2023; Accepted 2 August, 2023

The need for more bandwidth for a broad range of purposes necessitates research into how radio refractivity, multipath fading, and geoclimatic variables affect terrestrial and satellite propagation links. In this study, a geographical distribution approach to radio refractivity and fade depth over five locations in Nigeria—Akure, Enugu, Jos, Minna, and Sokoto based on five-year (2017–2021) measured data of atmospheric pressure, relative humidity, and temperature—at two levels (ground surface and 100 m heights). The results demonstrated the percentage occurrence of the dry terms dominating the radio refractivity constituent at the surface level, with a minimum and maximum contributions of about 78 and 92%, while at heights of 100 m, the percentage occurrence of the dry terms dominated the radio refractivity constituent, contributing a minimum of about 79% and a maximum of about 92%. The spatial distribution reveals that, regardless of height, the tropical rainforest (TRF) and freshwater swampy mangrove (FWSM) regions reported the highest values of radio refractivity. The statistical estimate shows that fading values can differ by as much as 1.5 dB, especially near the TRF and FWSM coastlines, even during clear air conditions. The current findings will be helpful for budgeting Earth-space microwave links, particularly for the rollout 5G and future-generation microcellular networks in Nigeria.

**Key words:** Geo-spatial distributions, Fade depth, Geoclimatic factor, Radio refractivity, Microwave applications

## **INTRODUCTION**

The modern world certainly yearns for greater change on a regular basis, which is why services that use radio and satellite telecommunication networks need more bandwidth. Most modern technical equipment benefits from faster data transmission speeds, reduced antenna sizes, higher throughput, and a wider band spectrum at higher frequencies, to name just a few (Hall, 1980;

Ippolito, 2008). However, the key concern for system designers to address, particularly at higher frequency bands, has been the worsening of propagation signals via space and terrestrial networks (Ojo, 2011).

The features of the earth and atmosphere have an impact on how electromagnetic waves travel around the planet, which induces fade depth (ITU-R 834-9, 2017;

E-mail: lojo@unilag.edu.ng

Author(s) agree that this article remain permanently open access under the terms of the [Creative Commons Attribution License 4.0 International License](https://creativecommons.org/licenses/by/4.0/)

Ojo and Ojo, 2018). The fade depth is the decibel-level (dB) difference between the power of a reference signal and the power during a fade. The reference value might already be known, such as the clear-sky value, which is frequently calculated as the averaged clear-air value. However, it is essential to investigate unusual microwave events that arise due to variations in climatological factors along the path of radio wave propagation in the troposphere in order to provide uninterrupted service.

Temperature, pressure, humidity, and particle density are examples of atmospheric variables that change across time and space. The interaction of these variables leads to the variation of radio refractive index in the troposphere. Adediji and Ajewole (2008) and Ojo et al. (2014) both observed that  $\mu$ wave systems could become unavailable due to seasonal variation of refractive index. Hence, precise information on the radio refractive index (time and space) in the troposphere is important in the planning and design of point-to-point radio links for  $\mu$ wave networks and other propagation applications. Although the world charts and global numerical maps provided by the International Telecommunication Union (ITU) are recommended for radio refractive index data, especially where local data are not available, research shows that such data does not perform well in Nigeria because the model that provided the data does not include data from this region (Igwe and Adimula, 2009; Adediji et al., 2014b). Hence, one of the objectives of this paper is to generate atmospheric radio refractivity data for wireless services and populate the ITU databank. Clear-air fading is also a result of the refraction of electromagnetic waves along the curvature of the earth in diverse directions. Atmospheric multipath, scintillation, ducting, and surface multipath are just a few of the clear-air mechanisms. When the direct beam and surface-reflected beam of signals merge, multipath fading happens (ITU-R 530-14, 2012). According to ITU guidelines, the design goal for fixed links is to achieve 99.99% service availability in the critical (worst) months of the year, implying an annual outage of no more than 53 min (Bogucki and Wielowieyska, 2009). Fading phenomena are a function of specific meteorological conditions, as reported by Asiyo and Afullo (2013). The method for calculating the percentage of time that a particular fade depth is exceeded relies on path length, frequency, and geoclimatic parameters; thus, it is imperative to estimate the fade depth for each site and area of interest. Some researchers in the tropical region, particularly in Nigeria, have made attempts to model the primary radioclimatic variables. Some of the attempts are, Falodun and Ajewole (2006), Igwe and Adimula (2009), Adediji et al. (2011), Oyedum (2012), Adediji et al. (2014a, 2014b), Ojo et al. (2014), and Falodun et al. (2021a, 2021b), to mention but a few. The present study's focus is on the estimation of fade depth for various outage probabilities and the associated Geoclimatic factors based on the radioclimatological data.

Since the required design fade margin is based on a precise computation of the intensity of fading events, radio link design is dependent on this information. When compared to median conditions, this is the level of signal loss that can be tolerated before major transmission mistakes happen. Despite the cost of raising the system fade tolerance due to things like larger antennas and more robust support systems, inadequate fade margin results in poor link error performance. In order to achieve optimum performance of terrestrial microwave links for the rollout of 5G networks and for other technologies depending on the required capacity and bandwidth in Nigeria, it is necessary to further study the distributions of radio refractivity and the effect of signal fading (Olla et al., 2019; Salamon et al., 2020).

## METHODOLOGY

The characteristics of the study locations, the instrumentation and the data analysis are presented in this section.

### The Nigeria climate

Nigeria (9° 04' 39.90 "N; 8° 40' 38.84 "E) is a country in West Africa located between the Sahel to the north and the Gulf of Guinea to the south in the Atlantic Ocean. The country covers a total area of about 923,769 km<sup>2</sup>. It is regarded as the most populous country in Africa. Depending on location, the country has a tropical climate with varying rainy and dry seasons. The southeast experiences hot, humid weather for the majority of the year, whereas the southwest and further interior experience dry weather. Particularly in the north and west, the northern region is characterized by a savanna climate with wet and dry seasons, while the extreme north is characterized by a steppe environment with low precipitation. The duration of the rainy season often shortens as we travel northward. For instance, whereas the rainy season only lasts from mid-May to September in the extreme north, it lasts from March to November in the southern portion. The so-called "August break" is always characterized by a brief dry spell and a pause in August rains in the southern region. While the far north only gets approximately 500 mm of rain per year, the southern section of the country receives greater amounts of rain, especially in the southeast, with about 3,000 mm of rain annually and 1,800 mm in the southwest (Hannaford and Beck, 2021).

Particularly in the southern hemisphere, temperature and humidity are largely stable year-round, but in the north, these variables change greatly. The average monthly maximum temperature along the shore is about 32°C, and the average monthly lowest temperature is about 21°C. The north experiences higher mean maximum temperatures of about 38 degrees Celsius during the warm months of April and May. In the north, the humidity is typically high; however, there is a slight reduction as the hot-dry northeast trade wind prevails (Eruola et al., 2021). Each of the study locations was chosen to represent the climatic region of the country, which spans from the southern to the northern parts. The locations were also selected based on the availability of the setup for in-situ measurements. The features of the study areas are presented in Table 1.

### Description of the instrument and data acquisition

For measuring the meteorological data (temperature, relative humidity, and atmospheric pressure) at the ground and 100 m at

**Table 1.** Features of the study sites.

Location	Climatic region	Coordinate (Degree)	Altitude (m)	Annual Mean Precipitation (mm)	Average Temperature (°C)
Akure	Tropical Rain Forest (TRF)	5°.12"E, 7°.15"N	358	1485.57	27.1
Enugu	Fresh Water Swap Mangrove (FWSM)	7°.27"E, 6°.25"N	223	1876.30	26.7
Minna	Guinea Savannah (GS)	6°.33"E, 9°.36"N	281	1196.75	27.0
Jos	Dense Savannah Woodland (DSW)	8°.53"E, 9°.55"N	1400	1186.89	23.0
Sokoto	Sudan Savannah (SS)	5°.13"E, 13°.04"N	500	567.21	28.3

Source: Ojo and Ojo, 2018

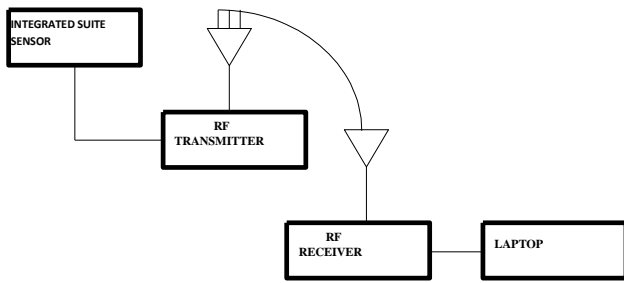


**Figure 1.** A schematic diagram of the equipment set up.  
Source: Adediji et al., 2007

the research locations, the integrated sensor suites (ISSs) are placed at a high mast. The equipment is available all year round in Akure, Enugu, Minna, Jos, and Sokoto for 97, 95, 93, 94 and 92%, respectively. The remainder of the time that equipment is unavailable is because of maintenance, which includes battery replacement. The technique used in this study allows for the precise determination of the variables needed for the estimate of the radio refractivity and its gradient at a precise height. By using this technique, the console is placed on the ground, and the sensors are mounted high on the tower. Radio waves are used to communicate the sensor signals to the receiver (console). The information is kept on the data logger that is connected to the ground-level console, and it is regularly copied and stored on the computer (the setting is unique at all the sites). Detailed descriptions of the equipment and measurements are available in the work of Ojo et al. (2015) and are not repeated here for the sake of space. Figure 1 shows a typical block diagram of the equipment set up at each of the sites. For the purpose of this study, each of the sites provided archived data of in-situ readings of the temperatures, pressures, and relative humidity. The data were obtained at Sokoto, Minna, Nsukka, Jos, and Akure sites for the surface (~ 65 m) and 100 m height for a period of 5 years (January 2017 to December 2021). Based on a total of about 24540 samples gathered, the recordings span 24 h each day from the first hours of the day to 2300 h local time at a 30 minute integration time. The values of pressure (hpa), relative humidity (%), and temperature (°C) were used as the primary climatic factors from the daily records of data obtained to derive the secondary and tertiary climatic-related variables.

### Data analysis

The earth's atmosphere is dynamic, which causes its characteristics

to change with changes in temperature, pressure, and humidity. These metrics, called primary climatic variables in relation to radio refractivity,  $N$ , were directly recorded from each of the sites (Freeman, 1997):

$$N = (n - 1)10^6 = \frac{77.6P}{T} + 3 \times 10^5 \frac{e}{T^2} = N_d + N_w \quad (1)$$

The parameter  $n$  represents the atmospheric refractive index;  $P$  denotes the atmospheric pressure measured in hpa;  $T$  denoted the temperature in Kelvin; and the water vapor pressure is referred to as  $e$  (hPa). The dry and wet parts of  $N$  are denoted  $N_d$  and  $N_w$ .  $e$  is related to the relative humidity  $H$  and the atmospheric saturation water pressure  $e_s$ , with only the air temperature  $t^\circ C$  reported in the work of Olsen and Tjelta (1999):

$$e = H \times \frac{6.1121 \exp\left(\frac{17.502T}{t+240.97}\right)}{100} \quad (2)$$

The height-related radio refractivity known as the gradient of the refractivity gradient in the atmosphere determines the level of fading emanating from different paths and can be expressed as:

$$\frac{dN}{dh} = \frac{N_1 - N_2}{h_1 - h_2} \quad (3)$$

In equation (3),  $N_1$  and  $N_2$  are the radio refractivity at the surface ( $h_1$ ) and 100 m height ( $h_2$ ), respectively.  $dN_1$ , known as the point radio refractivity at a point,  $dN_1$  is obtained from the  $N_1$ , and the radio refractivity within 1 km of the surface. Given that there is no data at precise heights, the following methodology is used (Dominguez et al., 1998):

$$dN_1 = \frac{N_1 - N_2}{h_1 - h_2} \quad (4)$$

In this case,  $h_1$  is the point close to 1 km height and  $dN_1$  is estimated only if  $900 \text{ m} < h_1 < 1100 \text{ m}$ . The procedure developed in ITU-R. P. 530-18 (2021) can be used to calculate the geoclimatic factor,  $K$  (for quick planning), where  $dN_1$  is the point refractivity gradient in the base 100 m (~ 65 m) of the atmosphere (as extracted in the measured data) that is not surpassed for 1% of an average year and is defined in this work as:

$$K = 10^{-4.2 - 0.0029 dN_1} \quad (5)$$

The worst month of the year for a pre-defined threshold for any performance degrading mechanism is the month throughout a

period of twelve continuous calendar months in which the threshold is surpassed for the longest period of time. Additionally, it should be noted that not all threshold levels' worst months are always the same month (Al-Ansari and Kamel, 2008; Olsen, 1999). According to the ITU P.530-18 (2021) recommendation, the following techniques can be used to estimate the narrow-band fading distribution at significant fade depths in the usual worst month for both quick planning and thorough planning purposes: the Geoclimatic factor  $K$  will initially be obtained, followed by the degree of the path inclination, and finally the percentage at which a specific fade depth  $A$  surpasses the mean worst month is determined.

The parameter  $K$  can be estimated using equations (5), while the path inclination ( $\eta$ ) can be estimated from the information on transmit and receive antenna heights  $h_t$  and  $h_r$  (m), above sea level and the path length  $d$  (km) from (ITU.R P.530-18, 2021):

$$|\eta| = \frac{|h_t - h_r|}{d} \tag{6}$$

Finally, the percentage of time  $P_w$  that a specific fade depth  $A$  (dB) exceeds the mean worst month is estimated using:

$$P_w = Kd^{3.0}(1 + |\eta|)^{-1.29}10^{-0.0033f - 0.001h_L - A/10} \tag{7}$$

where  $f$  denotes the frequency (GHz),  $h_L$  is the altitude of the lower antenna (the smaller of  $h_t$  and  $h_r$ ),  $d$  and  $K$  are the path length and geoclimatic factor, respectively. Knowing the likelihood that a fade depth of a specific magnitude will occur could directly affect the probability that an interruption will occur and, as a result, the possibility that the link will be available. This is because the propagation medium is varied. This is presuming that the received signal declines below the squelch level as a result of the preset fade depth (Bogucki and Wielowieyska, 2009). Table 2 presents the parameters of the sites used in estimating the fade depth.

The ordinary Kriging spatial interpolation technique (OKSIT) was used to determine the spatial distribution of radio refractivity and other secondary climatology variables. According to Cressie (1993), when all of the prerequisites for a certain type of Kriging are satisfied, it is the best linear unbiased predictor, which makes it a popular tool for linear spatial interpolation. Prominent Kriging methods like the ordinary Kriging spatial interpolation technique (OKSIT) presume that the data has a stable but unknown mean as well as a fixed and well-known isotropic geometric variance that changes with distance (Matheron, 1963; Ojo, 2017). The OKSIT system can be presented as follows:

$$\begin{bmatrix} W_1 \\ \cdot \\ \cdot \\ \cdot \\ W_n \\ \mu \end{bmatrix} = \begin{bmatrix} \gamma_{1,1} & \dots & \gamma_{n,1} & 1 \\ \cdot & \cdot & \cdot & \cdot \\ \cdot & \dots & \cdot & \cdot \\ \cdot & \dots & \cdot & \cdot \\ \gamma_{1,n} & \dots & \gamma_{n,n} & 1 \\ 1 & \dots & 1 & 0 \end{bmatrix}^{-1} \begin{bmatrix} \gamma_{1,p} \\ \cdot \\ \cdot \\ \cdot \\ \gamma_{n,p} \\ 1 \end{bmatrix} \tag{8}$$

where  $w_1..w_n$  is a symbol for the weights that apply to the  $n$  data points. The terms  $\gamma_{ij}$  represent the expected semi-variogram (S-V) function  $\gamma$  values for the spacing between pairs of known points  $i$  and  $j$ , and  $\gamma_{i0}$  represent the predicted  $\gamma$  values for the ranges  $h(i,p)$  between known points and the resampling point. This is possible if the S-V function has a slope that is non-zero and, ideally, maximal at the origin.

In order to make the semi-variogram functions continuous for the

sake of this study, we selected the precise interpolation method, which forces the interpolated area to pass through the known areas. We employed the frequency of radio refractivity at sets of locations in each of the country's climatic regions to accomplish this. Also, the exponential function has been used in the form of:

$$\gamma(h) = \sigma^2 [1 - \exp(-h/h_0)] \tag{9}$$

where  $\sigma^2$  is the data variance, although the weights given by (8) are independent of the value of  $\sigma^2$ . Hence, the S-V function may be assigned to the data by changing one parameter,  $h_0$  in (9), to determine the minimum root mean square interpolation error, as proposed by cross-validation. The fixed average and covariance assumptions of OKSIT are met using the interrelationship of the topography and weather types in Nigeria. Hence, the best, linear unbiased predictor perfectly fits our model. The choice is also due to the fact that  $n$  is interpolated in terms of a few hundred or less values, and the Kriging has been restricted to a smaller number of local locations that represent each of the climatic regions in Nigeria (Ojo, 2017). Hence results generated can be generalized within the entire country and localities with similar climatic pattern.

## RESULTS AND DISCUSSION

Detailed results from the analyses and discussion of the output are presented in this section.

### Morphology of the radio refractivity profile

When developing terrestrial and wireless communications infrastructure, the effects of radio refractivity in the lower atmosphere cannot be understated. Because trans-horizon transmission frequently leads to interference and multi-path fading if not properly accounted for. When it comes to the evaluation of radio refractivity, the influences of the wet and dry terms on the signal degradation, especially at frequencies above 30 MHz, are of concern, as indicated in equation (1). The wet and dry terms form the morphology of the radio refractivity and its gradient. The dry term makes up roughly 70% of the combined value of the refractivity, but the wet term is responsible for the majority of the fluctuation, according to Adediji et al. (2007). The wet term results from the polar character of the water molecules, whereas the dry term is related to the density of the gas molecules in the environment and varies with their concentration (Agunlejika and Raji, 2010). The wet term is related to vapor pressure and is dominated by the polar water content in the troposphere, whereas the dry term can be further simplified as being due to non-polar nitrogen and oxygen molecules. In other words, it relates to the air density since it is linked to the pressure, or  $P$ . Examining the spatial distributions of the two terms across Nigeria, their significance, and their impacts on microwave transmission deterioration are some of the objectives of this paper. The contributions can result in the occurrence of ducting and multipath conditions, especially at the lowest 100 m from the surface of the Earth used for

**Table 2.** Parameters for estimating fade depth (DVBS and S2, 2021).

S/N	Location	Frequency (GHz)	$h_t$ (m)	$h_r$ (m)	$h_L$ (m)	$d$ (km)
1	Akure	10 - 35	80	358	134	5-20
2	Enugu	10 - 35	100	223	100	5-20
3	Minna	10 - 35	50	281	50	5-20
4	Jos	10 - 35	165	1400	1400	5-20
5	Sokoto	10 - 35	185	500	185	5-20

Source: DVBS and S2, 2021

**Table 3.** Morphology of the radio refractivity over the study sites for dry season at the surface and 100 m heights.

Location	Climatic region	Average dry term	% contribution	Average wet term	% contribution
<b>Dry season (surface level)</b>					
Akure	(TRF)	256.18	77.97	72.38	22.03
Enugu	(FWSM)	276.62	77.93	78.35	22.07
Minna	(GS)	273.26	81.42	62.35	18.58
Jos	(GS)	273.92	82.44	58.35	17.56
Sokoto	(SS)	253.83	91.73	22.87	8.27
<b>Dry season (100 m)</b>					
Akure	(TRF)	251.21	79.17	33.14	10.45
Enugu	(FWSM)	297.41	81.34	68.25	18.67
Minna	(GS)	305.00	82.11	66.46	17.90
Jos	(DSW)	301.85	84.27	56.35	15.73
Sokoto	(SS)	257.98	91.47	24.90	8.83

**Table 4.** Morphology of the radio refractivity over the study sites for wet season at the surface and 100 m heights.

Location	Climatic region	Average dry term	% contribution	Average wet term	% contribution
<b>Wet Season (surface level)</b>					
Akure	(TRF)	260.16	70.39	111.26	29.54
Enugu	(FWSM)	211.69	61.69	131.45	38.31
Minna	(GS)	210.37	62.09	128.45	37.91
Jos	(DSW)	211.93	64.13	118.56	35.87
Sokoto	(SS)	253.22	70.26	107.17	29.74
<b>Wet Season (100 m)</b>					
Akure	(TRF)	259.88	71.00	108.89	29.00
Enugu	(FWSM)	239.50	63.37	138.46	36.63
Minna	(GS)	244.45	66.11	125.35	33.90
Jos	(DSW)	236.44	66.83	117.35	33.17
Sokoto	(SS)	269.43	73.92	93.30	26.90

microcellular propagation (ITU-R P.453-11, 2015). The percentage inputs of the dry and wet seasons for each site during the dry and wet seasons, for the surface and 100 m heights, are shown in Tables 3 and 4, respectively. Generating the mean-time proportion involves adding together each term's prediction and splitting by the total number of synoptic recordings.

Table 3 provides an overview of the expected morphological content of the radio refractivity at each site during the dry season. It is seen that the percentage occurrence of the dry terms dominated the constituent of the radio refractivity with a minimum contribution of about 78% and maximum contributions of about 92% at the surface level, while the dry terms dominated the radio

refractivity with a minimum contribution of about 79% and maximum contributions of about 92% at the 100 m heights. The percentage contribution of the wet terms varies between 8 and 22% at surface level, while it varies between 9 and 19% at 100 m height. Results from Table 3 also revealed that Sokoto, which belongs to the SS region, recorded the highest percentage contribution from the dry term and the lowest percentage contribution from the wet term. This should be expected since the SS region is associated with relatively high temperatures and pressures—the two major constituents of the dry terms. The FWSM region recorded the minimum percentage contribution from the dry term at the surface level. This might be due to the relatively cool temperatures recorded in the region. At 100 m, the SS region still had the highest percentage contribution, while the RF region had the lowest.

It should be noted that the present results do not agree with the general statement made by Adediji et al. (2007), which stated that the dry portion could be made up of about 70% of the total amount of radio refractivity in the atmosphere. The present study revealed the dynamics of the contributions based on different regions, and the contribution can be more than 90%. This is one of the benefits of studying the spatial distribution of dynamical parameters. However, the percentage contribution of the dry term component is still fairly stable, with the percentage contributions ranging between 78 and 92% at both surface and 100 m heights during the dry season. It must be noted that although the dry portion added the highest percentage value for the radio refractivity, the wet portion provided the main trend in the multipath fading of the microwave propagation systems. This is due to the constituents of water vapor and atmospheric humidity that attract more refraction and fading of electromagnetic waves. It may also result in the rapid fluctuation of microwave signals, regarded as scintillation (Agunlejika and Raji, 2010).

Table 4 also presents the morphology of the radio refractivity over the study sites for the wet season at the surface and 100 m heights. The same observation as that of Table 3 could be made, although with different results for the percentage contents of the dry and wet portions in different regions of the country. In general, the percentage contributions of the dry term are lower during the wet season when compared with those of the dry season. The percentage contribution ranges from 61.7 to 70.4% at surface level and from 63.4 to 73.9% at heights of 100 m. However, the percentage contributions of the wet terms are higher in the wet season than in the dry season due to the higher accumulation of water volume.

### **Monthly distributions of radio refractivity profile based on night and day-time**

The radio refractivity distributions during the day and

nighttime (06:00, 12:00, 18:00, and 00:00 h LT) are examined, and the results are presented in Figures 2(a) and (b) for the TRF site; Figures 3(a) and (b) for the FWSM chosen site; and Figures 4(a) and (b) for the GS chosen site, respectively. Figures 5(a) and (b) show the DSW selected site during the day, and Figures 6(a) and (b) show the SS selected site during the night. Each of the sites has been chosen to indicate the tropical vegetation in Nigeria. For example, Figures 2(a) and (b) display the monthly pattern of radio refractivity over the TRF region during the day and night, respectively. For instance, as displayed in Figure 2(a), the result reveals that for the TRF region, the low occurrence of radio refractivity is significant in February irrespective of the hours of the day and height, while radio refractivity attains maximum values in January at 6 h LT at both surface and 100 m. However, at noontime, it attains its peak in September during intense rainfall.

As shown in Figure 2(b), the night-time radio refractivity result further demonstrates that, for the TRF region, low values of radio refractivity are also prevalent in February, irrespective of the height. It shows that the possibility of ducting could be observed this month (although the result of the gradient of radio refractivity will better present it). However, radio refractivity attains peak values in the month of October at 18 h (surface and 100 m heights) and in December at 0.00 h in the night (surface and 100 m heights). These findings supported the dynamics of radio refractivity over time and in the months of the year. It is further proof that the FMWM (Figure 3) and DSW (Figure 5) regions' radio refractivity patterns are more comparable due to some shared environmental characteristics, although with different values of radio refractivity. When compared to other climatic zones taken into consideration for this work, both regions, for instance, have a considerable incidence of the average rainfall amount. It clearly demonstrates that Figure 1's pattern is totally different from other regions considered in this work. The TRF region exhibits clear and distinctive characteristics like high amounts of rainfall, being very hot and humid, and having very tall trees and shrubs like jungles, among others.

As shown in Figures 3 to 6, other climatic zones exhibit a similar pattern but with varying radio refractive index values and seasonal variations.

### **Spatial distributions of radio refractivity profile**

To obtain good coverage over Nigeria, other sites within the investigated geographical zones were also included in the contour map. Results are displayed as maps to clearly show the information required for link behavior under the dynamic pattern of the radio refractivity profile as well as the seasonal trend for each of the locations. The geo-spatial contours are produced using OKIT in a 2021 *MATLAB* program by incorporating the entire static

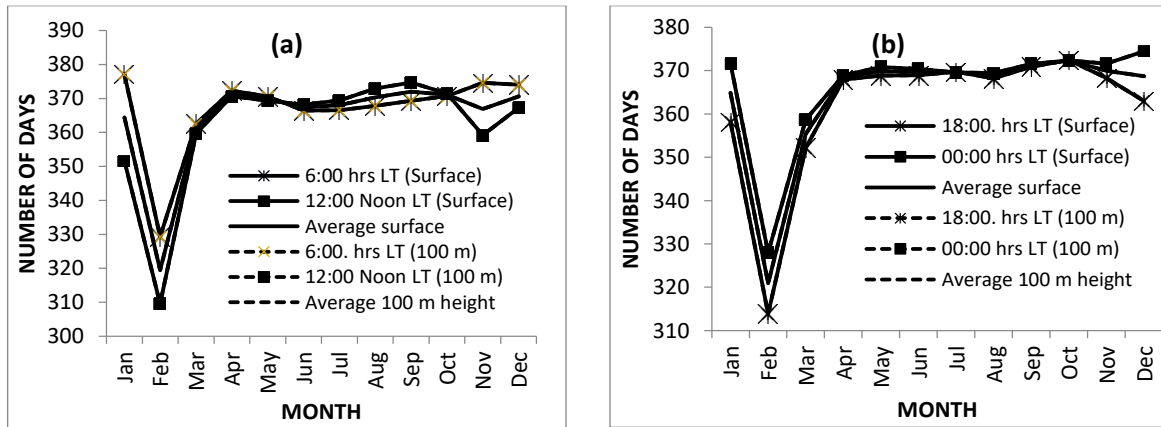


**Figure 2.** Monthly distribution of radio refractivity at surface and 100 m heights over TRF region during (a) daytime and (b) nighttime.

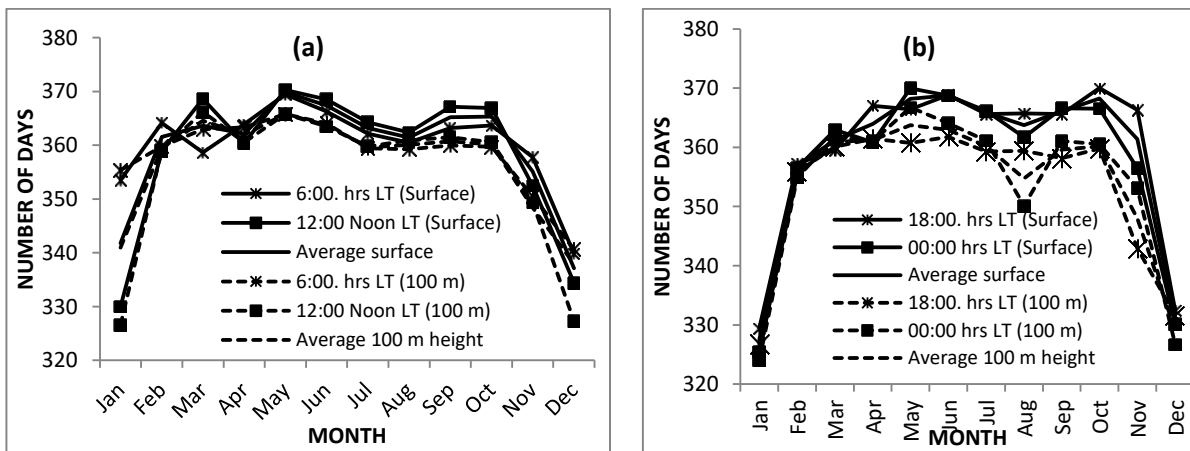


**Figure 3.** Monthly distribution of radio refractivity at surface and 100 m heights over FWFM region during (a) day-time and (b) night-time.

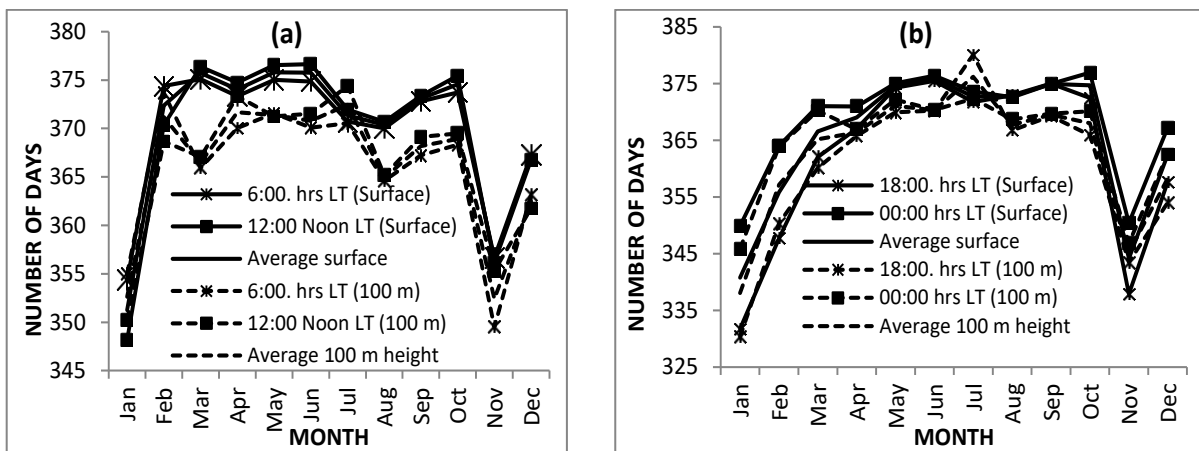


**Figure 4.** Monthly distribution of radio refractivity at surface and 100 m heights over GS region during (a):day-time and (b) night-time.

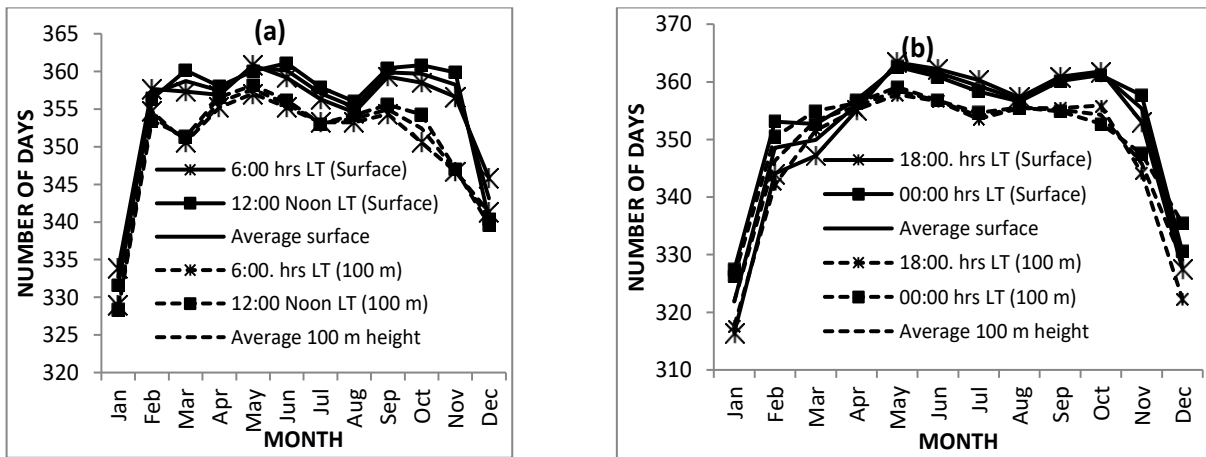


**Figure 5.** Monthly distribution of radio refractivity at surface and 100 m heights over DSW region during: (a) day-time and (b) night-time.

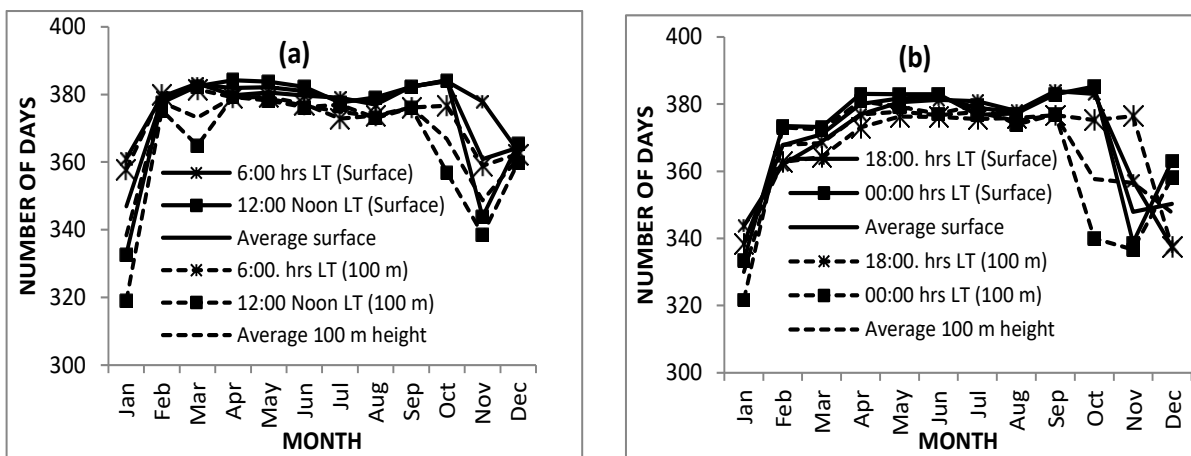


**Figure 6.** Monthly distribution of radio refractivity at surface and 100 m heights over SS (Jos) region during (a) day-time and (b) night-time.

but unknown mean and the static of a known isotropic spatial trend in equation (9) and the exponential function of equation (10) using the regulated grids. This will allow us to create a cross-functional and cross-radio refractivity profile difference that is highly reliable and consistent for any particular geographical area within the zone under consideration.

Figures 7a and b present the contour maps for radio refractivity over Nigeria at the surface level and at 100 m height, respectively. Based on the climatic features of each of the geographic areas, the curves on each map are designed differently. The surface radio refractivity in Figure 7a displayed more closely but spatially dense values with the TRF and FWSM zones, which are beside the riverside, producing a relatively wide difference in radio refractivity between locations with similar features.

This is demonstrated by the radio refractivity values, which in Enugu are about 365 N-units close to the seashore but drop to below 350 N-units for the Akure site as it rises above the sea, resulting in a severe variation in contour lines. It could also be seen from the maps that the TRF and FWSM regions of the country recorded the maximum values of radio refractivity irrespective of the height (Figure 7b). The northern areas of the country showed lower values of radio refractivity than the southern part, and contour lines covered a large area. In general, radio refractivity values were higher at the surface than at 100-meter heights. The fact that the ITU-R model underestimated radio refractivity values over Nigeria is clearly revealed with the help of these maps. It's possible that emission activities related to neighboring oil drilling are the cause of the decreased radio

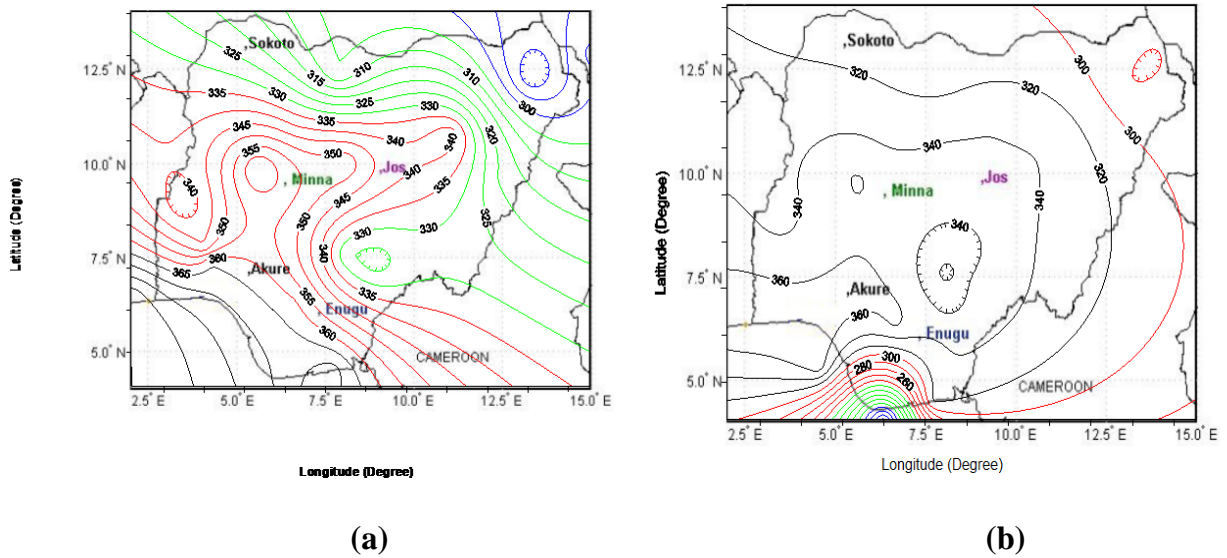
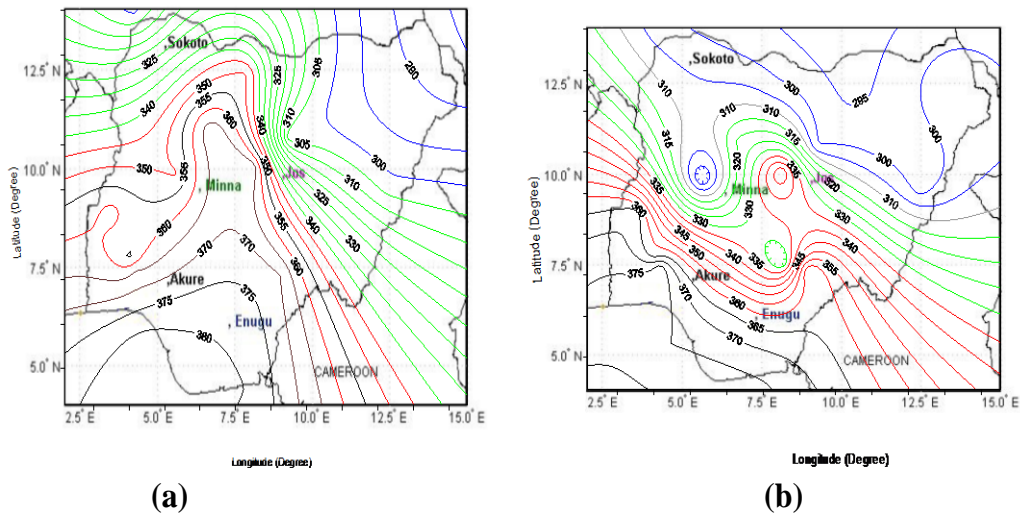


Figure 7. Contour map for average radio refractivity over Nigeria at the (a) surface and (b) 100 m height.



Figures 8. The contour maps for average radio refractivity over Nigeria (a) wet season and (b) dry season.

refractivity values exhibited in the southernmost portion of Figure 6b. As a result of the gas emissions that are occurring, carbon dioxide and sulfur dioxide are emitted into the atmosphere at a height of around 100 m. Figure 6b clearly depicts how these actions had an impact.

Figures 8a and b show contour maps for average radio refractivity over Nigeria (a) for the wet season and (b) for the dry season. It also shows that the TRF and FWSM regions of the country have the highest values of radio refractivity, irrespective of the seasons. The northern part

of the country shows lower values of radio refractivity than the southern part, irrespective of the seasons, because humidity is higher in the southern region of the country than in the northern zones. The contour lines widen along the TRF and FWSM shores (Enugu and Akure), but they retract towards the DSW and GS, which are territorially more rocky, and enlarge toward the SS area of the country, which is rather flat. These trends are also observed in the radio refractivity for the dry season maps, as presented in Figure 8(b). In general, radio

refractivity values were higher for the wet season as compared to the dry season.

The use of geospatial distribution analysis in wireless connection design budgeting underscores the importance of the maps, particularly for the deployment of 5G and proposed 6G microcellular networks in Nigeria. In order to reduce the effects of ducting and interfering, it will also allow radio access designers to account for the degree of multipath signal degradation by spreading the generated energy (down-link or up-link) (Ojo et al., 2017).

### **Fading due to Multipath exceeded for 1% of time at different path lengths**

When designing and performing wireless systems, understanding fading dynamics is crucial. The degree of signal distortion caused by the multipath intermittent attenuation of a microwave link is needed to establish a credible land-based link. It has been established that multipath fading is a random phenomenon that can only be described statistically (Olsen et al., 2003; Grami, 2016; Ashidi et al., 2020). On the basis of path lengths, fading phenomena can be predicted at a defined value of fade level or calculated at a specific percentage of outages. The ITU-R method can be used to estimate the fading caused by a fixed fade level at various path lengths. The percentage of times a specific fade depth is exceeded is predicted using the K values found in the preceding section.

The interruption that can occur at various scaling factors of fade depth at Ku and Ka-band frequencies are presented in this section. The Ku and Ka-band frequencies have been identified to address the concerns of rapidly expanding satellite broadband networks. There are initiatives to use Ka-band frequencies rather than Ku-band frequencies due to the Ku band's traffic and the capacity needs of the applications they are expected to support. Ka-band is also being thought about since Ku-band broadband networks using small dishes might encounter interruptions from terminals running on nearby satellites. Additionally, Ka-band standards demand faster return-link data throughput and a reduction of interference from surrounding satellites. This is the justification for selecting these frequency ranges. Equations (5)–(7) require link parameters, and in this analysis, the parameters used for the study locations have been presented in Table 2.

According to IEEE Standard 521 (2019), the fade depth is estimated for operating frequencies between the Ku downlink and the Ka-band, namely 10, 15, 20, 25, 30, and 35 GHz. Results for the fading on microwave attributed to the fading level at 5–20 km in the chosen locations over Nigeria are shown in Table 5. The values are generally lower at Ku-band frequency and greater at Ka-band frequency, according to the fading channels that were observed over the sites. Additionally, it is clear from the results that the fading gets worse as the path length

gets longer. According to this, even under conditions of clear skies, the uplink frequencies in the Ka-band will be noticeably fading from the microwave channels.

According to the findings, even within the same climate zone, mostly at uplink Ka and Ka-band frequencies, fading values can vary up to approximately 1.5 dB, particularly near the TRF and FWSM shores, including during clear air conditions. These results were based on climatic classification and separate path intervals. This investigation also supported certain findings that Olla et al. (2019) had already made. According to the article, fading caused by multipath is often stronger in Nigeria's shorelines (FSMW and TRF) as opposed to the country's northern plains (SS), and at Ka-band, the deterioration could lead to significant issues for satellite communications, particularly in the coastal zone. The present study further reveals that additional dust particles in the SS region may add to the fading value, and the results may also be of concern to the system engineer in the region.

It is also seen from Table 5 that the fading that could be encountered at microwave paths exceeded for 1% of time over the TRF and coastline for 5–20 km path lengths ranges between 20.99 dB and 24.87 dB at Ku–Ka band frequencies (10–35 GHz) for Akure and between 21.25 and 25.11 dB at Enugu (FMWS). It has been noted in the past that changes in radio refractivity and geoclimatic conditions cause fluctuations in fading (Freeman, 1999; ITU-530-530-18, 2021). It is worth mentioning that the fading due to the clear air effect shows different patterns from the TRF region, which is characterized by high moisture content with more contributions from wet terms of radio refractivity, to the far arid SS northern region of the country, which has more dust particles and a high temperature. The data shown in Table 5 for all sites at frequencies between 10 and 35 GHz makes this very clear.

## **CONCLUSION**

Results on Geo-spatial distribution of radio refractivity and the influence of fade depth on microwave propagation signals over Nigeria have been presented. The results reveal that the percentage occurrence of the dry terms dominated the constituent of the radio refractivity with a minimum contribution of about 78% and maximum contributions of about 92% at the surface level, while the dry terms dominated the radio refractivity with a minimum contribution of about 79% and maximum contributions of about 92% at the 100 m heights. Results from monthly distributions shows that surface radio refractivity is spatially distributed across Nigeria. The TRF and FWSM zones, which are located near the shore, produce a considerably large variation in radio refractivity values when compared to sites at 100 m height. The statistical distribution reveals the radio refractivity values of about 365 N-units in Enugu near the sea shore, which

**Table 5.** Fading due to multipath of microwave propagation exceeded for 1% of time at different path lengths over Nigeria.

Station	Region	Frequency (GHz)	5 km	10 km	15 km	20 km
Akure	TRF	10	20.99	22.46	23.30	23.88
		15	21.19	22.66	23.49	24.08
		20	21.38	22.85	23.69	24.28
		25	21.58	23.05	23.89	24.48
		30	21.78	23.25	24.09	24.67
		35	21.98	23.45	24.29	24.87
Enugu	FWSM	10	21.25	22.71	23.55	24.12
		15	21.45	22.91	23.74	24.32
		20	21.65	23.11	23.94	24.52
		25	21.85	23.31	24.14	24.72
		30	22.06	23.52	24.35	24.93
		35	22.24	23.70	24.53	25.11
Minna	GS	10	21.25	22.71	23.55	24.12
		15	21.45	22.91	23.74	24.32
		20	21.65	23.11	23.94	24.52
		25	21.85	23.31	24.14	24.72
		30	22.05	23.50	24.34	24.92
		35	22.24	23.70	24.53	25.11
Jos	DSW	10	19.78	21.24	22.08	22.67
		15	19.98	21.44	22.28	22.86
		20	20.18	21.64	22.48	23.06
		25	20.38	21.84	22.68	23.26
		30	20.57	22.04	22.87	23.46
Sokoto	SS	10	20.86	22.32	23.16	23.75
		15	21.60	22.52	23.36	23.94
		20	21.26	22.72	23.56	24.14
		25	21.46	22.92	23.76	24.34
		30	21.65	23.12	23.95	24.54
		35	21.85	23.32	24.15	24.74

decrease to less than 350 N-units for the Akure location, which drifts away from the coasts, producing contour lines with a sharp inclination. It could also be seen from the maps that the TRF and FWSM regions of the country produced the highest results in radio refractivity, irrespective of their height. The values for the multipath-induced fading over the studied locations are lower at Ku-band frequencies and greater at Ka-band frequency. The results also show that the fading becomes worse as the route distance increases. This suggests that even in the presence of a clear sky, the microwave links' uplink frequencies in the Ka-band will be noticeably weakened. It further shows that fading values can differ by as much as 1.5 dB, especially near the TRF and FWSM coastlines, regardless of the presence of clear skies. However, more

locations across Nigeria over the V- and W-bands are suggested for future work with more years of measurement.

### CONFLICT OF INTERESTS

The author has not declared any conflict of interests.

### ACKNOWLEDGEMENTS

The National Space Research and Development Agency, the Federal Ministry of Science and Technology, Anyigba, and Nigeria's Centre for Atmospheric Research are acknowledged by the author for the data used in this

work. The author also appreciates the Federal Government of Nigeria for funding the Nigerian Space Program, as well as the Centre for Atmospheric Research and their partners for fostering high standards of atmospheric observatory operations ([www.carnasrda.com](http://www.carnasrda.com)). The effort of Professor J.S. Ojo in editing and proofreading the manuscript is also highly recognized.

## REFERENCES

- Adediji AT, Ajewole MO, Falodun SE, Oladosu OR (2007). Radio refractivity measurement at 150 m altitude on TV tower in Akure, South-West Nigeria. *Journal of Engineering and Applied Sciences* 2(8):1308-1313.
- Adediji AT, Ajewole MO, Falodun SE (2011). Distribution of radio refractivity gradient and effective earth radius factor (k-factor) over Akure South Western Nigeria. *Journal of Atmospheric and Solar Terrestrial Physics*. 73:2300-2304.
- Adediji AT, Mandeep JS, Ismail M (2014). Meteorological Characterization of Effective Earth Radius Factor (k-Factor) for Wireless Radio Link over Akure, Nigeria. *MAPAN-Journal of Metrology Society of India* 29(2):131-141.
- Adediji AT, Mahamod I, Mandeep JS (2014). Variation of radio field strength and radio horizon distance over three stations in Nigeria. *Journal of Atmospheric and Solar Terrestrial Physics* 109:1-6.
- Al-Ansari K, Kamel RA (2008). Correlation between ground refractivity and refractivity gradient and their statistical and worst month distribution in Abu Dhabi. *IEEE Antennas and Wireless Propagation Letters* 2:233-235.
- Agunlejika O, Raji TI (2010). Empirical evaluation of wet -term of refractivity in NIGERIA. *International Journal of Engineering and Applied Sciences* 2(2):63-68.
- Ashidi A, Ojo JS, Adediji AT, Ajewole MO (2020). Development and performance evaluation of tropospheric scintillation model on Ku-band satellite link over Akure, Nigeria. *Advances in Space* 67(5):1612-1622.
- Asiyu MO, Afullo JO (2013). Statistical Estimation of Fade Depth and Outage Probability Due to Multipath Propagation in Southern Africa. *Progress in Electromagnetics Research* 46:251-274.
- Bogucki J, Wielowiejska E (2009). Empirical season's fading's in radio communication at 6 GHz band. *Journal of Telecommunications and Information Technology* 2:48-52.
- Cressie NAC (1993). "Spatial prediction and Kriging, 'in Statistics for Spatial Data. New York, NY, USA: Wiley pp. 105-210.
- Dominguez MA, Benarroch A, Riera JM (1998). Refractivity Statistics in Spain: First Results. Tech. Rep. CP52004, COST 255 p.
- DVBS S2 (2021). Digital Video Broadcasting (DVB); Second generation framing structure, channel coding and modulation systems for Broadcasting, Interactive Services.
- Eruola AO, Makinde AA, Eruola GA, Ayoola KO (2021). Assessment of the Rainfall Exceedance in Nigeria. *Nigerian Journal of Technology* 40(4):751-761.
- Falodun SE, Ajewole MO (2006). Radio refractivity index in the lowest 100 m layer of the troposphere in Akure, South-western Nigeria. *Journal of Atmospheric and Solar-terrestrial Physics* 68:236-243.
- Falodun SE, Ojo JS, Aboyeji ST (2021). Modeling of atmospheric primary Radioclimatic variables in Nigeria for microwave radio propagation applications. *SN Applied Sciences* 3:67.
- Falodun SE, Ojo JS, Kareem AI (2021). The Study of Atmospheric Stability Using Radio Refractivity Profiles over a Tropical Climate in Nigeria. *MAPAN* 36:751-762
- Freeman RL (1997). Radio System Design for Telecommunications. John Wiley & Sons, ISBN :978-0-471-75713-9.
- Grami A (2016). Book chapter Chapter 12 – Introduction to Digital Communications, Science Direct book pp. 493-527.
- Hall MPM(1989). Effect of the Troposphere on Radio Communication. IEEE Electromagnetic Wave Series, Peter Peregrinus Ltd, Stevenage pp. 105-116.
- Hannaford MJ, Beck KK (2021). Rainfall variability in southeast and west-central Africa during the Little Ice Age: do documentary and proxy records agree?. *Climatic Change* 168:11.
- Igwe KC, Adimula IA (2009). Variation of surface radio refractivity and radio refractive index gradients in the Sub-Sahel. *Nig. Journal of Space Research* 6:135-144.
- ITU- Rec P.453-8, (2003).The radio refractive index: Its formula and refractivity data.
- ITU-R P.530-14, (2012). Propagation data and prediction methods required for the design of terrestrial line-of-sight systems.
- ITU-R P.453-11, (2015). Radio Refractive Index: its formula and refractivity data" Rec. P 453-11, International Telecommunication Union, Geneva (2015).
- ITU-R P.834-9, (2015). Effects of tropospheric refraction on radiowave propagation" Rec. P 834-9, International Telecommunication Union, Geneva (2017).
- Matheron G (1963). Principles of Geostatistics. *Economic geology* 58(8):1246–1266.
- Salamon SJ, Hansen HJ, Abbott D (2020). Universal Kriging Prediction of Line-of-Sight Microwave Fading. *IEEE Access* 8:74743-74758.
- Olla MO, Oluwafemi IB, Akinsanmi O, Femijemilohun OJ (2019): Fade Depth and Outage Probability Due to Multipath Propagation in Nigeria. *Research Journal of Applied Sciences, Engineering and Technology* 16(2):43-55.
- Ojo JS (2011): "Rain rate statistics and fade distribution at Ka-and Ku band frequencies for microwave propagation in tropical locations" *The Nigerian Journal of Space Research* 10:72-80.
- Ojo JS (2017). Geo-spatial distribution of cloud cover and influence of cloud induced attenuation and noise temperature on satellite signal propagation over Nigeria. *Advances in Space Research* 59:2611-2622
- Ojo JS, Ajewole MO, Obagunle RG (2017). Performance of Site Diversity Fade Mitigation over Earth to Space Propagation Link using Rain Cell Measurements in a Tropical Nigeria- IET Microwave, Antenna and propagation. 11(15):2260-2266.
- Ojo OL, Ajewole MO, Adediji AT, Ojo JS (2014). Microwave Anomalous Propagation Conditions in the First 100-m Altitude in a Tropical Location. *Journal of Microwave Power and Electromagnetic Energy*. 48(2):131-137.
- Ojo OL, Ojo JS (2018). Analysis of Clear Air Effects: Implication on Microwave Radio Systems in Nigeria. *Advances in Research* 14(5):1-8.
- Olsen RL (1999). Radioclimatological Modeling of Propagation Effects in Clear-Air and Precipitation Conditions: Recent Advances and Future Directions. *Proceedings of the Third Regional Workshop on Radio Communications in Africa Radio Africa '99, Gaborone, Botswana.*
- Olsen RL, Tjelta (1999). Worldwide techniques for predicting the multipath fading distribution on terrestrial LOS links: Background and results of tests. *IEEE Transactions on Antennas and Propagation*, 47(1):157-170
- Olsen RL, Tjelta T, Martin L, Segal B (2003). Worldwide techniques for predicting the multipath fading distribution on terrestrial LOS links: Comparison with regional techniques. *IEEE Transactions on Antennas and Propagation* 51(1):23-30
- Oyedum OD (2012). Duct-Induced terrestrial microwave link degradation in Nigeria: Minimization factors, *India Journal of Radio and Space Physics* 41:339-347.